JOURNAL OF AIRCRAFT
Vol. 47, No. 3, May–June 2010

Self-Sustained Oscillations of Turbulent Flow in an Open Cavity

Sang Bong Lee,* Abu Seena,† and Hyung Jin Sung‡
Korea Advanced Institute of Science and Technology, Daejeon 305-701, Republic of Korea

DOI: 10.2514/1.44823

Direct numerical and large eddy simulations of incompressible turbulent flows over deep and shallow cavities were performed in the range of $600 \leq Re_D \leq 12,000$ to investigate the influence of the incoming turbulent boundary layer on self-sustained oscillations of the shear layer. When the turbulent boundary layer approached the open cavity with $Re_D = 3000$, the energy spectra of the pressure fluctuations showed spectral peaks in the range of $0.15 \leq \omega_\theta \leq 0.3$. Conditionally averaged flowfields disclosed that the spectral peaks arise from the separation of high-speed streaky structures rather than from a geometric singularity of the cavity. The same spectral peaks were observed in a backward-facing step flow as well as in deep and shallow cavity flows, despite the different geometries of these systems. In the turbulent cavity flow of $Re_D = 12,000$, however, the peak frequencies of the energy spectra at cavity lengths of $L/D = 1$ and 2 were found to correspond to the Nth modes with $N = 2$ and 3, respectively. These Nth modes were very similar to the frequency characteristics of self-sustained oscillations reported for laminar cavity flows. Inspection of instantaneous pressure fluctuations as well as spanwise-averaged pressure fluctuations revealed that regular shedding of quasi-two-dimensional vortical structures was responsible for the peak frequency in the energy spectra.

Nomenclature

D	=	cavity depth
L	=	cavity length
N	=	oscillation mode
Re_D	=	Reynolds number, $U_\infty D/\nu$
Re_θ	=	Reynolds number, $U_\infty \theta/\nu$
$R_{\varphi\varphi}$	=	two-point correlation
St_D	=	Strouhl number, fD/U_∞
U_C	=	convection velocity
U_∞	=	freestream velocity
δ	=	boundary-layer thickness
δ_ω	=	vorticity thickness
θ	=	momentum thickness of incoming boundary layer
κ_z	=	spanwise wave number
λ_x	=	streamwise wavelength
ω_θ	=	angular velocity of fluctuations
$+$	=	normalized by wall unit
$\langle\,\rangle$	=	operator of conditional averaging

I. Introduction

FLOWS over open cavities occur in many engineering applications, for example, landing gear wells and bomb bays in aircraft and sunroofs in automobiles. The presence of the open cavity generates strong self-sustained oscillations of velocity, pressure, and, occasionally, density, which may induce strong vibrations in the substrate over which the fluid is flowing, which may give rise to structural fatigue or acoustic noise. To understand the mechanism underlying such oscillations and prevent undesirable effects, numerous experimental and numerical studies have been carried out since Norton [1] investigated the buffeting of bomber airplanes due to airflow over their bomb bays.

Rossiter [2] investigated the influence of cavity dimensions and freestream velocity on oscillating behavior and proposed an empirical equation to predict the oscillation frequency in compressible flows with sub- and transonic Mach numbers. Ahuja and Mendosa [3] carried out wind-tunnel experiments to study the effects of incoming boundary-layer characteristics on acoustic tones and found that the intensity of the resonant oscillations diminishes with increasing incoming boundary-layer thickness. Many numerical simulations have shown that the self-sustained oscillations of compressible flows arise due to a resonance between shear layer instabilities and acoustic disturbances [4,5]. This resonance is based on a feedback mechanism, whereby small disturbances in the shear layer are amplified due to the Kelvin–Helmholtz instability. When the small disturbances impinge on the trailing edge of the cavity, strong pressure fluctuations propagate upstream to the leading edge and disturb the separated shear layer.

Although the mechanism of self-sustained oscillations has been well characterized for compressible flows, the hydrodynamic oscillations of incompressible flows over an open cavity have received less attention. Sarohia [6] found that, for a laminar incoming boundary layer, the self-sustained oscillations occur under the criterion of $L/\delta(Re_\delta)^{1/2} > 290$ and the oscillating frequency jumps to a higher mode as the cavity length increases. Gharib and Roshko [7] identified two oscillation modes in laminar cavity flows, which they denoted "shear layer mode" and "wake mode." When the ratio of the cavity length to the incoming boundary-layer momentum thickness (L/θ) exceeds 80, the self-sustained oscillations are in the shear layer mode. When the ratio exceeds 120, however, the oscillations shift to the wake mode, causing an abrupt increase in the drag. Many other studies of incompressible flows over an open cavity support the notion that the incoming laminar boundary layer can generate self-sustained oscillations due to shear layer instabilities [8–12].

When the incoming boundary layer is turbulent, however, it is unclear whether the turbulent incoming boundary layer can give rise to self-sustained oscillations [9]. Pereira and Sousa [13] observed periodically oscillating shear layers in the flow of a turbulent incoming boundary layer over an open cavity. Lin and Rockwell [14] also observed self-sustained oscillations in water-tunnel experiments and suggested that the oscillations are related to large-scale vortical structures. In contrast, Grace et al. [15] found no evidence of self-sustained oscillations in velocity and pressure data from their

Received 13 April 2009; revision received 7 August 2009; accepted for publication 11 August 2009.

*Professor, Department of Mechanical Engineering, 373-1 Guseong-dong, Yuseong-gu.
†Ph.D. Student, Department of Mechanical Engineering, 373-1 Guseong-dong, Yuseong-gu.
‡Ph.D. Student, Department of Mechanical Engineering, 373-1 Guseong-dong, Yuseong-gu; hjsung@kaist.ac.kr. (Corresponding Author).

experiment with a turbulent incoming boundary layer. Chatellier et al. [16] observed self-sustained oscillations of the mixing layer in their experiments and theoretically analyzed the fluctuating behaviors of turbulent cavity flows at low Mach numbers. They suggested that the oscillating process is not governed by periodic shedding of coherent structures but by convective waves of the naturally unstable mixing layer. However, Ashcroft and Zhang [17] observed the shedding of large-scale vortical structures by Galilean decomposition of the instantaneous and fluctuating velocity fields. The coherent vortical structures were present in the majority of particle image velocimetry images, although well-defined structures were not always observed. The authors pointed out small peaks in the pressure spectra as evidence of weak tonal components; however, strong self-sustained oscillations were not observed.

Previous studies of incompressible flows over an open cavity have been predominantly experimental investigations, with only a relatively small number of numerical simulations. Pereira and Sousa [13] performed numerical simulations of unsteady incompressible Navier–Stokes equations, but their simulations were confined to two dimensions. Recently, Chang et al. [18] performed large eddy simulations (LESs) under the same flow conditions as those of Pereira and Sousa [13]. They found that, whereas regular shedding of vortical structures was responsible for self-sustained oscillations in laminar flows, no shedding of quasi two-dimensional vortical structures was observed in turbulent flows. In the turbulent system, the power spectra of the vertical velocity component were broad, with energy-containing frequencies up to $St < 1.0$. Considering that the self-sustained oscillations of laminar cavity flow take place at large L/θ, the momentum thickness of the incoming boundary layer is too thick to reveal whether the incoming turbulent boundary layer can generate self-sustained oscillations. Specifically, the turbulent case was simulated under the condition of $L/\theta = 7.2$, whereas the ratio was 69.5 for the laminar case.

As reviewed above, the existence of self-sustained oscillations has not been conclusive yet in incompressible turbulent cavity flows. In previous experiments, it has been difficult to determine the occurrence of hydrodynamic oscillations in incompressible turbulent cavity flows because the oscillations are very weak due to both the absence of acoustic resonance and the fluctuations of upstream turbulence. In previous numerical studies, three-dimensional direct numerical simulation (DNS) of incompressible turbulent cavity flows has not been performed at high Reynolds numbers of large L/θ due to the prohibitive cost of computations. In the present study, we performed DNSs and LESs of incompressible turbulent flows over deep and shallow cavities for a wide range of Reynolds numbers ($600 \le Re_D \le 12,000$), where Re_D is the Reynolds number based on the cavity depth. The present simulations used L/θ values of up to 80, which is sufficiently large to identify the existence of self-sustained oscillations. The turbulent flow over a backward-facing step was also simulated for comparison. Based on the numerical results, it was elucidated whether a fully turbulent boundary layer can give rise to self-sustained oscillations in incompressible cavity flows. In the incompressible turbulent flows over an open cavity of small L/θ, the influence of near-wall turbulent structures on the behavior of separated shear layers was examined. When the incoming turbulent flows approached the cavity geometry of large L/θ, the relation between the oscillations and coherent vortex formations was scrutinized. To analyze the fluctuating behaviors of the turbulent cavity flows in detail, turbulence statistics and frequency spectra of fluctuating quantities were obtained. Conditional averaging and spanwise averaging were employed to extract spatial maps of the pressure fluctuations.

II. Numerical Method

For an incompressible flow, the nondimensional governing equations are

$$\frac{\partial u_i}{\partial t} + \frac{\partial u_i u_j}{\partial x_j} = -\frac{\partial p}{\partial x_i} + \frac{1}{Re_D}\frac{\partial^2 u_i}{\partial x_j^2}, \qquad i = 1, 2, 3 \tag{1}$$

$$\frac{\partial u_i}{\partial x_i} = 0 \tag{2}$$

where x_i are the Cartesian coordinates and u_i are the corresponding velocity components. The freestream velocity (U_∞) and the cavity depth (D) are used for nondimensionalization. The Reynolds number is defined as $Re_D = U_\infty D/\nu$, where ν is the kinematic viscosity. The governing Eqs. (1) and (2) are integrated in time using the fully implicit decoupling method proposed by Kim et al. [19]. All terms are advanced in time with the Crank–Nicholson method and are resolved with the second-order central difference scheme in space. Based on a block lower–upper triangular decomposition, both velocity–pressure decoupling and additional decoupling of the intermediate velocity components are achieved in conjunction with the approximate factorization. The multigrid method is applied to obtain the solution of the pressure Poisson equation in a T-shaped domain.

A schematic diagram of the computational domain is shown in Fig. 1. For all of the present simulations, the turbulent boundary layer was provided at the inlet with the realistic velocity fluctuations of $Re_\theta = 300$, which were generated using the method of Lund et al. [20]. Their method was to recycle the turbulent velocity profile from a station downstream and reintroduce the profile as the inflow boundary condition. The inflow calculations of the present study made use of $65 \times 74 \times 129$ grid points in the domain of $(L_x, L_y, L_z) = (80\theta, 30\theta, 40\theta)$. The momentum thickness Reynolds number at the inflow plane was fixed at $Re_\theta = 280$. The recycle station was located 64θ downstream of the inlet. Other parameters of weighting function have been well documented in the previous study of Lund et al. [20]. After saving the velocity data at the plane of $Re_\theta = 300$ in the inflow simulation, data were provided at the inlet when the main simulations of turbulent cavity flows were performed. The convective outflow condition $\frac{\partial u_i}{\partial t} + U_c \frac{\partial u_i}{\partial x_i} = 0$ is used at the exit, where U_c is the convection velocity. A no-slip boundary condition is imposed at the solid wall. Neumann conditions are imposed at the freestream, and periodic boundary conditions are used in the spanwise direction.

DNSs of incompressible flows over an open cavity were performed for two Reynolds numbers, $Re_D = 600$ and 3000. The cavity flows at a high Reynolds number ($Re_D = 12,000$) were simulated using an LES with a dynamic subgrid-scale model [21]. The simulation conditions used in the present study are summarized in Table 1. The infinity symbol (∞) represents turbulent flows over a backward-facing step. N_t is the number of grid points in each direction, and the mesh resolutions are nondimensionalized by the friction velocity of the incoming turbulent boundary layer (u_τ). $\Delta x^+_{\min}$ and $\Delta x^+_{\max}$ represent the mesh resolutions at the trailing edge and outlet, respectively. Uniform grids were used in the spanwise direction. Nonuniform grids were used in the streamwise and wall-normal directions, with higher densities of grid points near the leading and trailing edges. As the cavity length was increased, the number of grid points in the streamwise direction was increased to keep the mesh resolution constant. The sizes of $\Delta x^+_{\min}$ and $\Delta y^+_{\min}$ were determined by obtaining the convergence of turbulent intensities near the wall and the trailing edge. The computational time steps are free from the CFL limit by using the fully implicit decoupling method. The time step was fixed at $\Delta t = 0.05D/U_\infty$ for

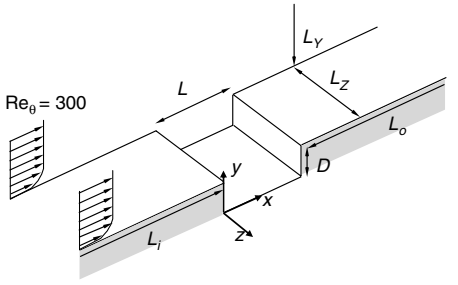

Fig. 1 Schematic diagram of the computational domain.

Table 1 Simulation conditions

Re_D	$L/D, L/\theta$	$N_x \times N_y \times N_z$	$\Delta x^+_{\min}, \Delta x^+_{\max}$	$\Delta y^+_{\min}$	Δz^+	$T_{\text{avg}} D/U_\infty$	L_Z/D
600	1, 2	$289 \times 95 \times 129$	0.80, 8.9	0.18	5	500	20
	2, 4	$321 \times 95 \times 129$	0.80, 8.9	0.18	5	500	20
3000	1, 10	$417 \times 133 \times 129$	1.12, 18	0.18	5	210	4
	2, 20	$513 \times 133 \times 129$	1.11, 18	0.18	5	210	4
	4, 40	$705 \times 133 \times 129$	1.04, 18	0.18	5	180	4
	6, 60	$897 \times 133 \times 129$	1.11, 18	0.18	5	180	4
	∞, ∞	$577 \times 133 \times 129$	1.88, 18	0.18	5	210	4
12,000	1, 40	$705 \times 169 \times 257$	1.4, 40	0.56	10	110	4
	2, 80	$897 \times 169 \times 257$	1.4, 40	0.56	10	103.125	4

$Re_D = 600$, whereas $\Delta t = 0.004D/U_\infty$ or $0.007D/U_\infty$ was used for $Re_D = 3000$. For $Re_D = 12,000$, the time step was very small such as $\Delta t = 0.001875D/U_\infty$ due to the explicit characteristics of dynamic subgrid-scale model. After a long initial transient period due to the large residence time of fluid particles in the recirculation zone, the stochastic data were averaged in time (T_{avg}) as well as in the homogeneous spanwise direction. The initial transient time of more than 10 "flow through" was discarded to allow for the passage of unphysical fluctuations, whereas the "flow through" time is defined as the convection time through the full domain at the mean convection speed, $0.6 \sim 0.8U_\infty$.

The computational domain size was determined after checking two-point correlations of velocity fluctuations. The domain size in the spanwise direction (L_Z) was 4 times the cavity depth (D) for $Re_D = 3000$ and 12,000 and $20D$ for $Re_D = 600$. These spanwise domain sizes are supported by the results of previous numerical simulations of turbulent flows over a backward-facing step [22]. The domain size in the streamwise direction was $L_i = L_o = 19D$ for $Re_D = 600$, $L_i = L_o = 9D$ for $Re_D = 3000$, and $L_i = 4D$ and $L_o = 7.5D$ for $Re_D = 12,000$, respectively. Here, L_i and L_o are the streamwise lengths of the development section before the leading edge and after the trailing edge, respectively. The postexpansion length of the backward-facing step was set to $20D$, which is sufficient to describe the downstream development of vortical structures. The vertical height (L_Y) was set to greater than $15D$ for $Re_D = 600$ and the height was $5D$ for $Re_D = 3000$ and 12,000. The Neumann boundary imposed at the freestream was sufficiently far from the free shear layer of the turbulent cavity flow to allow the turbulent intensity to monotonically decrease to a constant value.

III. Identification of Pressure Fluctuations

Before examining in detail whether self-sustained oscillations exist, it is helpful to compare the characteristics of the pressure fluctuations (p') observed in the turbulent cavity flows at the three Reynolds numbers. Figure 2 shows the energy spectra of the pressure fluctuations at $(x/D, y/D) = (0.5, 1.0)$ for length-to-depth ratios (L/D) of 1 and 2. The energy spectra of the systems with $Re_D = 600$, 3000, and 12,000 are shown in Figs. 2a–2c, respectively. The frequency is nondimensionalized by using the momentum thickness of the incoming turbulent boundary layer, that is, $\omega_\theta = 2\pi f\theta/U_\infty$. Spectral peaks are observed in all of the spectra, although the pressure fluctuations at $Re_D = 600$ show broad spectra due to small energetic increases. As shown in Figs. 2a and 2b, the pressure fluctuations are energetic in the frequency range of $0.15 \le \omega_\theta \le 0.3$, regardless of the length-to-depth ratio. This suggests that the energetic pressure fluctuations observed for the $Re_D = 600$ and 3000 systems are little affected by the geometrical dimensions of the cavity. In the $Re_D = 12,000$ spectra (Fig. 2c), however, the peak in the fluctuation spectrum shifts to lower frequency as the cavity length increases. Specifically, the frequency range exhibiting energetic pressure fluctuations is $0.15 \le \omega_\theta \le 0.2$ for $L/D = 1$, but about 0.08–0.12 for $L/D = 2$. This frequency shift in the fluctuation spectrum as a function of cavity length is very similar to the previous observation that, as the cavity length was increased, the frequency of self-sustained oscillations in a system with a laminar incoming boundary layer decreased [7].

To characterize the pressure fluctuations in the frequency range around the peak in the energy spectrum, a more instructive view can be derived by examining the temporal evolution of the fluctuation

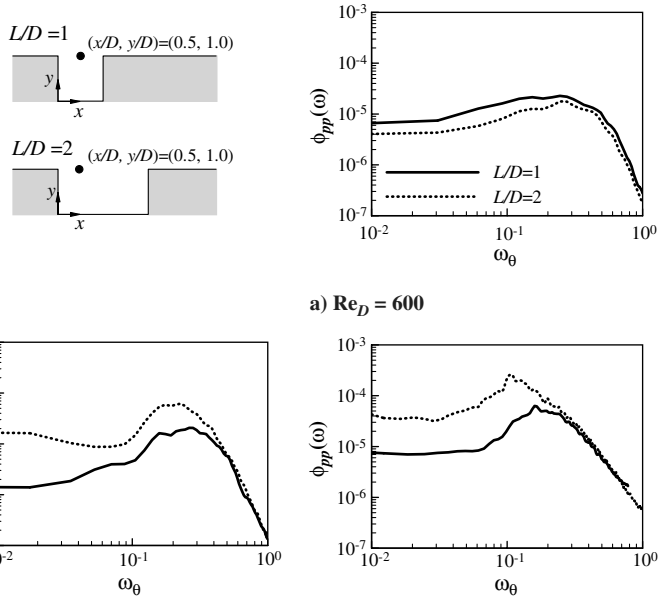

Fig. 2 Energy spectra of pressure fluctuations measured at $(x/D, y/D) = (0.5, 1.0)$.

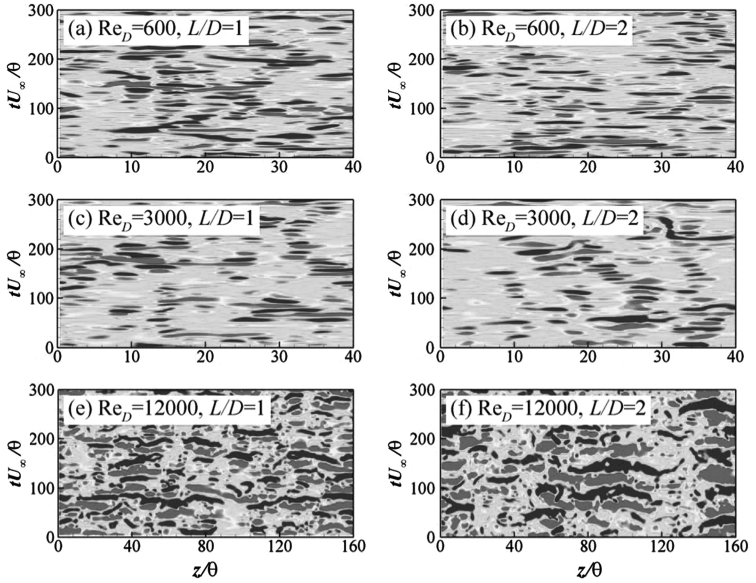

Fig. 3 Time histories of pressure fluctuations corresponding to the energy spectra of Fig. 2. Spanwise length and time are normalized by the momentum thickness of the incoming turbulent boundary layer (θ).

distribution in the spanwise direction. Figure 3 shows such time histories in which the horizontal and vertical axes represent the spanwise direction and time, respectively, and the pressure fluctuations corresponding to the energy spectra of Fig. 2 are represented on a gray scale. Close inspection of Fig. 3 discloses that the pressure fluctuations in the $Re_D = 600$ and 3000 systems (Figs. 3a–3d) exhibit qualitatively different characteristics from those in the $Re_D = 12,000$ system (Figs. 3e and 3f). Specifically, at $Re_D = 600$ and 3000, the pressure undergoes three-dimensional fluctuations intermittently. At $Re_D = 12,000$, by contrast, quasi-two-dimensional pressure fluctuations are regularly observed, albeit with slight variations away from two-dimensional behavior. Note that the spanwise length scale of Figs. 3e and 3f is 4 times longer than that of Figs. 3a–3d. A detailed comparison of the $Re_D = 12,000$ systems with $L/D = 1$ and 2 (Figs. 3e and 3f, respectively) indicates that the time scale of the pressure fluctuations increases with increasing cavity length. This finding is consistent with the dependence of spectral peaks on cavity length shown in the energy spectra of the $Re_D = 12,000$ system. Based on the above examination of the energy spectra and their time evolution at different Reynolds numbers, we can identify two regimes of pressure fluctuations in incompressible turbulent flows over an open cavity. At lower Reynolds numbers, the pressure undergoes three-dimensional fluctuations intermittently and the frequency region with intense pressure fluctuations is insensitive to the cavity dimensions. At higher Reynolds number, quasi-two-dimensional pressure fluctuations are regularly observed and the frequency region with energetic fluctuations shifts to lower frequency as the cavity length increases. To determine whether the energetic pressure fluctuations of each regime can be regarded as self-sustained oscillations, it is necessary to identify coherent structures that are responsible for the energetic pressure fluctuations. In the following sections, we analyze the cavity flows at $Re_D = 3000$ and 12,000 to scrutinize the pressure fluctuation characteristics in the first and second regimes, respectively.

IV. Flow Characteristics at $Re_D = 3000$

A. Time-Mean Characteristics

Figures 4a–4d show the time-averaged streamlines of turbulent flows over deep and shallow cavities, whereas Fig. 4e shows the streamlines of the flow over a backward-facing step for comparison. When the length-to-depth ratio is unity (Fig. 4a), the mean flow is characterized by a primary vortex on the order of the cavity size. When the cavity length is increased to $L/D = 2$ (Fig. 4b), however, the primary vortex elongates up to the trailing edge of the cavity and a

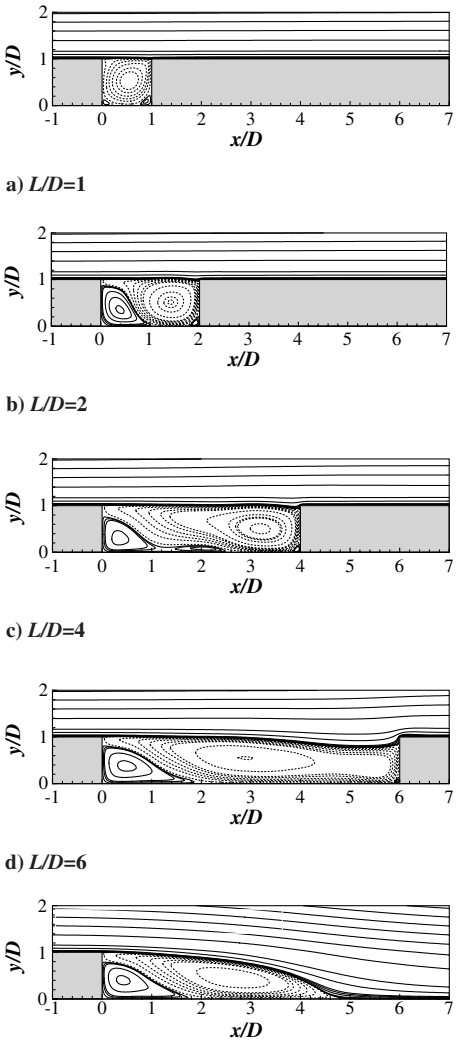

Fig. 4 Mean flow streamlines.

Table 2 Locations of the primary vortex core

Re_D	L/D	$(x/D, y/D)$
3000	1	(0.55, 0.55)
	2	(1.42, 0.51)
	4	(3.20, 0.50)
	6	(2.91, 0.55)
	∞	(2.63, 0.44)
Pereira and Sousa [13]		(1.42, 0.53)
Chang et al. [18]		(1.42, 0.52)

secondary vortex appears in the upstream region of the cavity. The sizes and relative positions of the primary and secondary vortices in the $L/D = 2$ cavity are very similar to the mean streamlines reported by Chang et al. [18] for the case of turbulent flow over an open cavity and the experimental visualizations of such systems reported by Pereira and Sousa [13]. The Reynolds number of the previous numerical and experimental studies ($Re_D = 3360$) is similar to the present Reynolds number of $Re_D = 3000$. In the case of $L/D = 2$ reported here, as well as in the previous studies, the core of the primary vortex is located at $(x/D, y/D) = (1.42, 0.51 \sim 0.53)$, as listed in Table 2. The primary vortex core moves downstream when the length-to-depth ratio is further increased to 4, but moves back upstream slightly when the length-to-depth ratio is increased to 6. The behavior of the primary vortex core suggests that the cavity flow is likely to resemble the backward-facing step flow for length-to-depth ratios greater than 6.

B. Spectral Characteristics

To examine the spectral characteristics at a length-to-depth ratio of unity and $Re_D = 3000$, we determined the frequency spectra of the velocity and pressure fluctuations at four representative streamwise locations between the leading edge ($x/D = 0$) and the trailing edge ($x/D = 1$), the region immediately downstream of the leading edge ($x/D = 0.05$), the center of the cavity ($x/D = 0.5$ and 0.75), and the impingement region near the trailing edge ($x/D = 0.95$). The four locations are placed on the lip line ($y/D = 1$) of the cavity geometry. For a length-to-depth ratio of unity, no spectral peaks are observed in the spectra of streamwise velocity fluctuations (u') (Fig. 5a). The spectra of the vertical and spanwise velocity fluctuations show spectral peaks, although the energetic increases are very small (Figs. 5b and 5c). In the spectra of the pressure fluctuations, however, spectral peaks are clearly observed between $\omega_\theta = 0.15$ and 0.3 (Fig. 5d). This range is converted to $0.24 \le St_D \le 0.5$ using $St_D = fD/U_\infty$, which is consistent with the previous observation of slightly more intense pressure fluctuations at the frequencies of $St_D = 0.38$ and 0.51 [18]. Although these previous findings were obtained for $L/D = 2$ rather than $L/D = 1$, the consistency between the present and past results is reasonable because the spectral peaks are constant in the energy spectra of $L/D = 1$ and 2, as shown in Fig. 2. Our findings also show that no frequency range with enhanced pressure fluctuations is observed in the impingement region near the trailing edge ($x/D = 0.95$ data in Fig. 5d). This lack of peak frequencies in the pressure spectrum of the impingement region as well as in the spectra of streamwise velocity fluctuations is very important, because it indicates that the fluctuating behavior of cavity flows may be missed if wall pressure fluctuations or velocity fluctuations are measured only at the trailing edge at the lip line ($y/D = 1$) of the cavity geometry.

The energy spectra in Fig. 5 raise two questions: Why are spectral peaks observed in the frequency spectra of pressure fluctuations? And why are no spectral peaks evident in the pressure spectrum of the impingement region as well as in the spectra of streamwise velocity fluctuations? To answer the first question, we examined in detail the time evolution of the pressure fluctuations at $(x/D, y/D) = (0.5, 1.0)$ at locations along the spanwise direction, as shown in Fig. 6. Figure 6 shows parts of Fig. 3c, in which the horizontal and vertical axes represent the spanwise direction and time, respectively. Both time and spanwise length are nondimensionalized by using the momentum thickness of the incoming turbulent boundary layer, that is, tU_∞/θ and z/θ. As discussed in Sec. III and shown in Fig. 6, the pressures show intermittent three-dimensional fluctuations with periods between 20 and 30. The range of the periods is in accord with the spectral peaks of the pressure spectra ($0.15 \le \omega_\theta \le 0.3$). This indicates that the intermittent strong fluctuations in the pressure are responsible for the spectral peaks.

To show the coherent structures that generate the intermittent pressure fluctuations, the instantaneous flows were conditionally averaged. By analyzing the full time histories of the pressure fluctuations at $(x/D, y/D) = (0.5, 1.0)$, we identified the points on the map of time versus spanwise location where the pressure fluctuations were a local minimum satisfying $p' < -1.5p_{\rm rms}$ or a local maximum satisfying $p' > +1.5p_{\rm rms}$. For example, in Fig. 6, the white and black circles represent the local minima and maxima identified in this way, respectively. At each time point, the

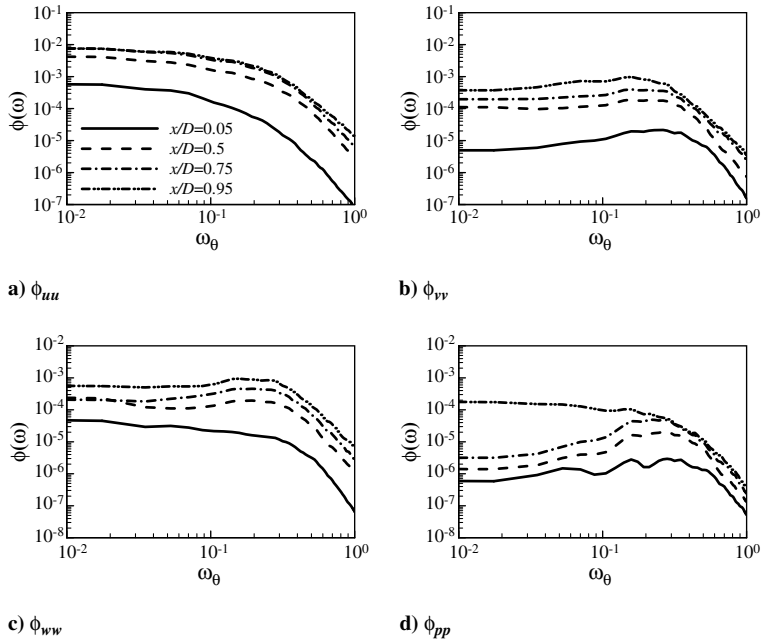

Fig. 5 Energy spectra of fluctuating quantities at four streamwise locations between the leading edge ($x/D = 0$) and the trailing edge ($x/D = 1$). The length-to-depth ratio is unity and $Re_D = 3000$.

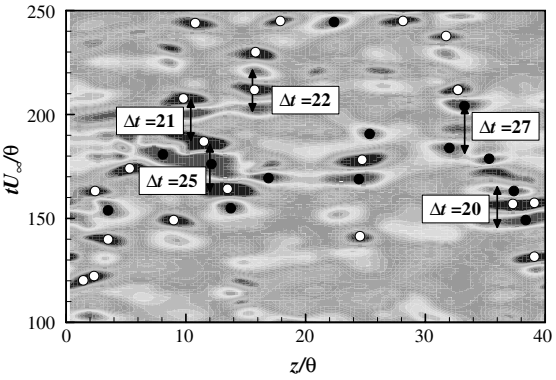

Fig. 6 Time histories of pressure fluctuations measured at $(x/D, y/D) = (0.5, 1.0)$ when the length-to-depth ratio is unity. The white and black circles represent local minimum points satisfying $p' < -1.5p_{\text{rms}}$ and local maximum points satisfying $p' > +1.5p_{\text{rms}}$ respectively.

instantaneous flow was averaged around the spanwise locations. Figure 7a shows the contour plot of the pressure fluctuations and the vector plot of the velocity fluctuations in the lip plane under the conditions of local minimum and $p' < -1.5p_{\text{rms}}$, whereas Fig. 7c displays a two-dimensional plot on the cutoff plane of Fig. 7a. The black contours and dotted lines represent negative pressure fluctuations whereas the gray contours and solid lines represent positive pressure fluctuations. As seen in Figs. 7a and 7c, the counterclockwise rotating vectors represent a vortical structure with strong negative pressure fluctuations. This structure has length scales of $\Delta x/D = 0.4 \sim 0.5$ in the streamwise direction and $\Delta z/D \leq 1$ in the spanwise direction. Figure 7b shows three-dimensional pressure fluctuations averaged under the condition of local maximum and $p' > +1.5p_{\text{rms}}$, whereas Fig. 7d displays the two-dimensional plot on the cutoff plane of Fig. 7b. These representations show that positive pressure fluctuations occur between two vortical structures. The vortical structure near the leading edge has just been generated and the other vortical structure is likely to impinge on the trailing edge. The positive pressure fluctuations are interpreted as being induced by the two vortical structures, as observed in the vortical shedding of a separated shear layer [23]. Moreover, the strong negative pressure fluctuations of the vortical structures and the induced positive pressure fluctuations are responsible for the intermittent pressure fluctuations.

As seen in Figs. 7a–7d, the positive fluctuations of streamwise velocity ($u' > 0$) occur near the leading edge and in the vicinity of the center along the lip line of the cavity geometry. It is interesting to note that the vertical distribution of u' is very similar to that of the incoming turbulent boundary layer. For example, the maximum fluctuations are observed near $y/D = 1.07$ (Figs. 7c and 7d), which exactly correspond to $y^+ \approx 12$ of the turbulent boundary layer, where the streamwise velocity fluctuations are most intense. It is expected that the positive streamwise velocity fluctuations observed over the cavity represent high-speed streaky structures of the incoming turbulent boundary layer. Considering that the Kelvin–Helmholtz instability arises when the velocity difference between shear layers exceeds a certain level, it is natural that the high-speed streaky structures can make the separated shear layer locally unstable due to the large velocity difference. Visualization of snapshots of the flow supports the notion that the high-speed streaky structures of the incoming turbulent boundary layer play a significant role in the generation of the observed intermittent pressure fluctuations. Figure 8a displays a snapshot of the high-speed streaky structures (represented by showing only contours with $u' \geq 0.18U_\infty$) in the plane $y/D = 1$, whereas Fig. 8b shows a contour plot of the pressure fluctuations in the same plane. In Fig. 8b, the solid and dotted lines represent positive and negative pressure fluctuations, respectively. Comparison of Figs. 8a and 8b shows a strong correlation between the high-speed streaky structures and the regions of positive and negative pressure fluctuations, consistent with the high-speed streaky structures passing over the cavity generating the energetic pressure fluctuations with three dimensionality.

To determine why the spectral peaks of pressure fluctuations disappear in the impingement region near the trailing edge, we examined spanwise-wave-number–frequency (κ_z–ω_θ) spectra at four streamwise locations: $x/D = 0.05$, 0.5, 0.75, and 0.95 (Fig. 9). The

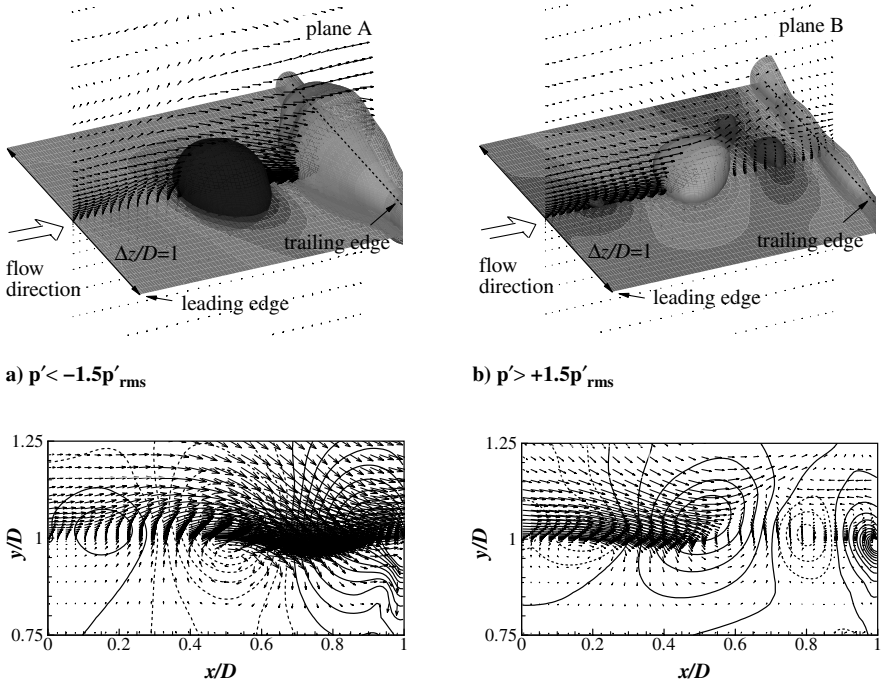

Fig. 7 Conditional-averaged contours of pressure fluctuations and vectors of velocity fluctuations: a) and c) instantaneous flows averaged under the conditions of local minimum pressure fluctuations satisfying $p' < -1.5p_{\text{rms}}$, and b) and d) instantaneous flows averaged under the conditions of local maximum pressure fluctuations satisfying $p' > 1.5p_{\text{rms}}$. The black contours and dotted lines represent negative pressure fluctuations whereas the gray contours and solid lines represent positive pressure fluctuations.

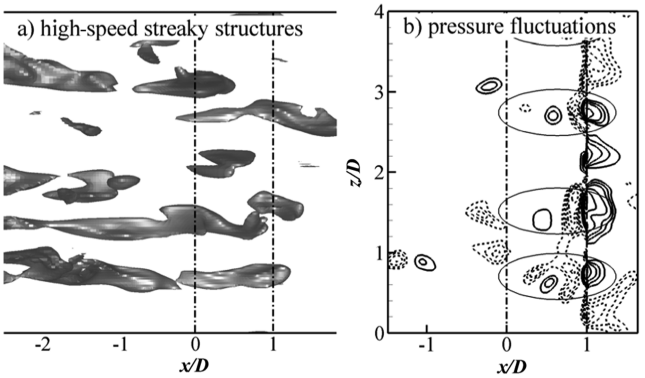

Fig. 8 Top view of instantaneous high-speed streaky structures and pressure fluctuations in the plane of $y/D = 1$. The high-speed streaky structures are represented by the contours of $u' = 0.18U_\infty$.

spanwise wave number and the frequency are nondimensionalized using the cavity depth and the momentum thickness of the incoming boundary layer, respectively. To facilitate comparison, the magnitudes of the energy spectra have been rescaled. We have already established that the high-speed streaky structures passing over the cavity generate the energetic pressure fluctuations in the frequency range of $0.15 \leq \omega_\theta \leq 0.3$, as indicated by "F mode" (i.e., fluctuating mode) in Figs. 9a–9c. In the κ_z–ω_θ spectrum for $x/D = 0.95$ (Fig. 9d), however, another energetic region appears, indicated by "I mode" (i.e., impinging mode), in addition to the F mode. These findings indicate that the F mode does exist in the impingement region, but that the energy-containing frequencies associated with this mode are buried in the energetic increases corresponding to the I mode. To elucidate the energetic increases of the I mode, which is observed only in the impingement region, we compared the probability densities of pressure fluctuations at two streamwise locations in the impingement region, $x/D = 0.95$ and 0.99, with those observed at $x/D = 0.05$ and 0.75 (Fig. 10). In these plots, the solid and dotted lines represent probability density functions (p.d.f.s) and weighted p.d.f.s, respectively. As shown in Figs. 10a and 10b, the distributions of both p.d.f.s and weighted p.d.f.s are almost symmetric, indicating that the negative and positive pressure fluctuations have the same characteristics in terms of the frequencies at which they appear. In the impingement region (Figs. 10c and 10d), however, the distributions are asymmetric, indicating that strong positive fluctuations ($p' > 2p_{\text{rms}}$) are more frequently observed than strong negative fluctuations ($p' < -2p_{\text{rms}}$).

The frequent appearance of strong positive fluctuations in the impingement region is confirmed in Fig. 11, which shows the instantaneous correlations between the streamwise velocity fluctuations (u') of three streamwise locations and the pressure fluctuations of the impingement region. The streamwise velocity fluctuations are measured at $y/D = 1.07$, which corresponds to $y^+ \approx 12$. As seen in Fig. 11, all negative pressure fluctuations fall between -0.1 and 0 ($-0.1 < p' < 0$), whereas positive pressure fluctuations larger than 0.1 are frequently observed. It is interesting to note that positive u' values are always observed between the leading and trailing edges whenever strong positive pressure fluctuations ($p' > 0.1$) are detected in the impingement region, as indicated by the circles in Fig. 11. The elongated regions of positive u' over the cavity represent the high-speed streaky structures of the incoming turbulent boundary layer. The behavior observed in Fig. 11 is consistent with Fig. 7b, which shows strong positive contours of pressure fluctuations on the trailing edge when the high-speed streaky structures pass over the cavity. The impingement of high-speed streaky structures generates strong positive pressure fluctuations near the trailing edge, which in turn increase the fluctuating energy of the I mode near the impingement region, thereby obscuring the energy-containing frequencies associated with the fluctuating mode.

Next, to determine why no spectral peaks are observed in the spectra of the streamwise velocity fluctuations, we examined two-point correlations of velocity and pressure fluctuations as a function of the streamwise distance (Fig. 12):

$$R_{\phi\phi}(\Delta x; X_0) = \frac{\langle \phi(X_0)\phi(X_0 + \Delta x)\rangle}{\phi_{\text{rms}}(X_0)\phi_{\text{rms}}(X_0 + \Delta x)} \tag{3}$$

Here, the angle bracket indicates an average over the spanwise direction and time. The correlations are calculated along the lip line of the cavity geometry by using the leading edge as a reference point, that is, the points of $\Delta x/D = 0$ and 1 represent the leading and

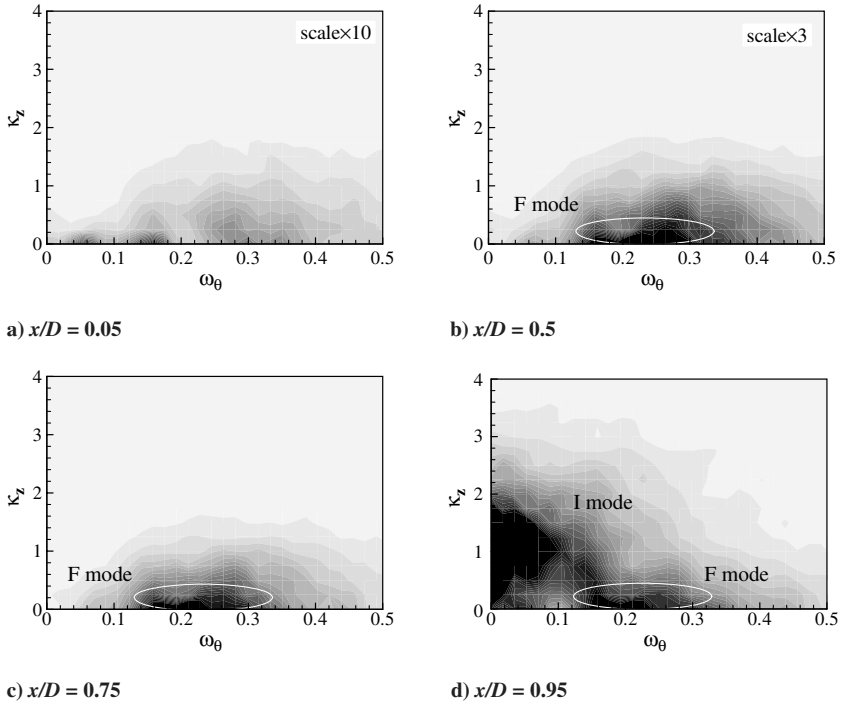

a) $x/D = 0.05$ **b) $x/D = 0.5$**

c) $x/D = 0.75$ **d) $x/D = 0.95$**

Fig. 9 Spanwise κ_z–ω_θ spectra at different streamwise locations. Here κ_z is normalized by using the cavity depth, whereas ω_θ is normalized by the momentum thickness of the incoming turbulent boundary layer.

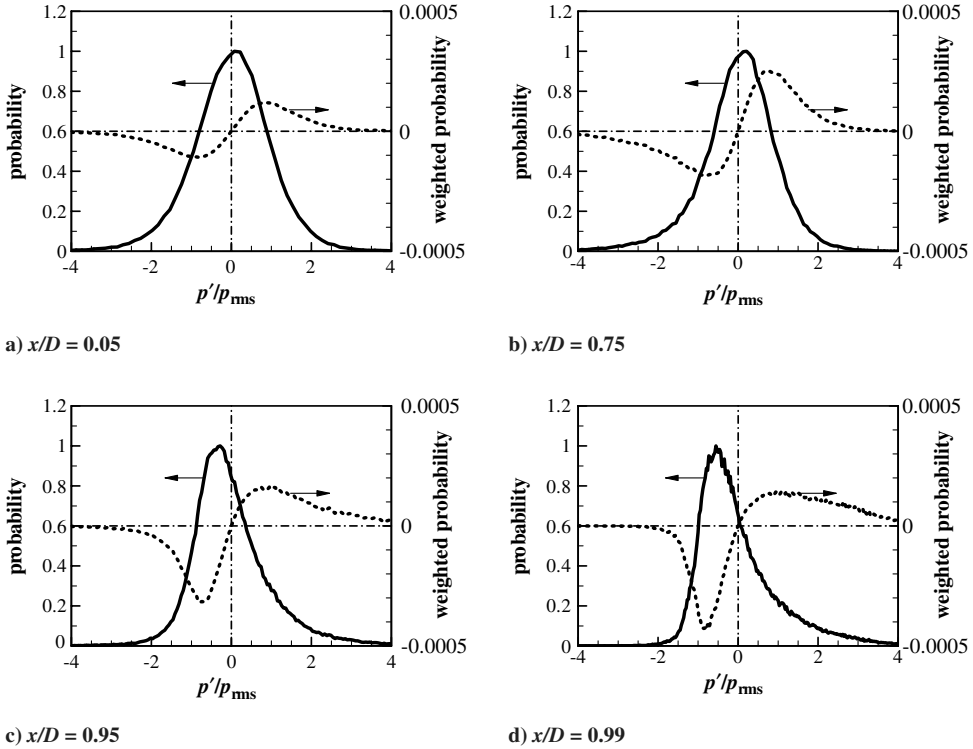

Fig. 10 Distributions of probability density functions and weighted probability density functions at different streamwise locations. The solid and dotted lines represent p.d.f.s and weighted p.d.f.s, respectively.

trailing edges of the cavity, respectively. As seen in Fig. 12, the correlations of pressure fluctuations fall off to negative values in the vicinity of $x/D = 0.5$ and then return to positive values near $\Delta x/D = 0.9$. The correlation data indicate that the vertical structures with negative pressure fluctuations induce positive pressure fluctuations and that these structures have length scales of $\Delta x/D = 0.4 \sim 0.5$ in the streamwise direction, as observed in Fig. 7. The correlations of vertical and spanwise velocity fluctuations as well as pressure fluctuations fall off to almost zero near the trailing edge. In contrast, the streamwise velocity fluctuations decrease monotonically when moving downstream and show strong correlations between the leading and trailing edges. These characteristics lead to the observation of no spectral peaks in the spectra of the streamwise velocity fluctuations. As a result, the streaky structures of the incoming turbulent boundary layer are little affected by the presence of the cavity.

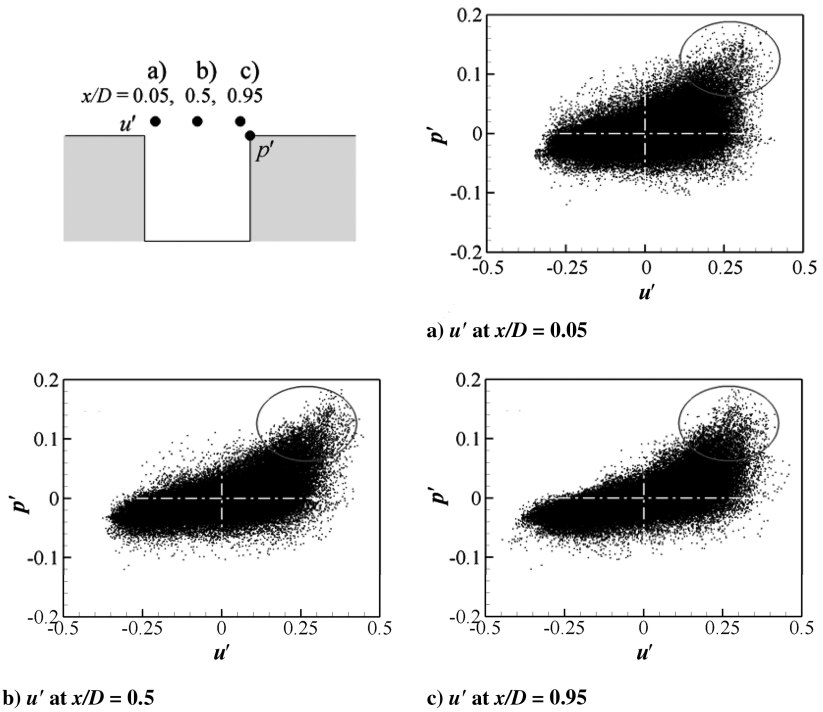

Fig. 11 Instantaneous correlations between the streamwise velocity fluctuations (u') of three different streamwise locations and the pressure fluctuations (p') of the trailing edge. The circles indicate that positive u' values are always observed between the leading and trailing edges whenever strong positive pressure fluctuations are detected in the impingement region.

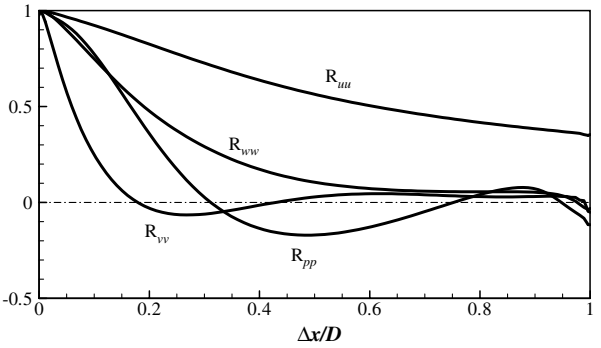

Fig. 12 Two-point correlations of velocity and pressure fluctuations in streamwise direction. The leading edge is used as a reference point.

C. Effect of Cavity Length on Pressure Fluctuations

Figure 13 shows the frequency spectra of pressure fluctuations for systems with cavity lengths of $L/D = 1$, 2, and 4. The pressure fluctuations are obtained at several streamwise locations between the leading and trailing edges along the lip line of the cavity geometry. Near the leading edge ($x/D = 0.5$), all spectra show spectral peaks in the range of $0.15 \leq \omega_\theta \leq 0.3$ regardless of the length-to-depth ratio. In the center of the $L/D = 1$ and 2 cavities (dotted lines in Figs. 13a and 13b, respectively), the spectral peaks are observed in the same range ($0.15 \leq \omega_\theta \leq 0.3$). In the center of the $L/D = 4$ cavity (dotted or dashed lines in Fig. 13c), however, the pressure fluctuations show energetic spectra at frequencies less than $\omega_\theta = 0.15$. Considering that the large-scale vortical shedding of the flow over a backward-facing step takes place in the vicinity of $\omega_\theta = 0.07$, as shown in Fig. 13d, large-scale vortical structures are likely to begin forming in the shallow $L/D = 4$ cavity, but the trailing edge impedes further development of those structures. The disrupting influence of the trailing edge leads to considerable variation in the large-scale vortical structures, and well-defined large structures are not regularly observed.

V. Flow Characteristics at $Re_D = 12,000$

A. Time-Mean Characteristics

Figure 14 shows the time-averaged streamlines at $Re_D = 3000$ and 12,000 for cavities with length-to-depth ratios of 1 and 2. For the $L/D = 1$ system, increasing the Reynolds number from $Re_D = 3000$ to 12,000 leads to the formation of a new vortex near the leading edge (Figs. 14a and 14b). For $L/D = 2$, the $Re_D = 3000$ to 12,000 flows exhibit different shapes of the secondary vortex in the upstream portion of the cavity (Figs. 14c and 14d). This difference in the shapes of the secondary vortex suggest that the behaviors of the separated shear layers in the $Re_D = 3000$ and 12,000 cavity flows will be quite different.

B. Spectral Characteristics

As mentioned in Sec. III, the pressure fluctuations in the $Re_D = 12,000$ system correspond to the "high Reynolds number regime," in which quasi-two-dimensional pressure fluctuations are regularly observed and the frequencies of energetic fluctuations decrease as the cavity length increases. Figure 15a shows the frequency spectra of pressure fluctuations in the $Re_D = 12,000$ cavity flows with length-to-depth ratios of 1 and 2. Here the pressure fluctuations are measured at $(x/D, y/D) = (0.5, 1.0)$ and the frequency is non-dimensionalized using the cavity depth, that is, $\omega = 2\pi f D/U_\infty$. The peak frequency of energetic pressure fluctuations decreases from $\omega_{\text{peak}} = 6.2$ to 4.5 as the cavity length increases. This decrease in peak frequency with increasing cavity length is very similar to the trend observed previously in the frequency of self-sustained oscillations in the flow over an open cavity with a laminar incoming boundary layer. Gharib and Roshko [7] found that the oscillating frequency of "mode II" decreased from 6 to 4 Hz as the length-to-depth ratio increased from 0.65 to 1.05, and that the shear layer oscillation shifted to "mode III" for ratios larger than 1.1. The oscillating frequencies of modes II and III are determined by the relation

$$L/\lambda_x = fL/U_C = N \tag{4}$$

where λ_x is the streamwise wavelength of oscillation, f is the oscillating frequency, U_C is the convection velocity, and N is the number of wavelengths of fundamental frequency contained by the cavity length in the Nth mode of oscillation. Equation (4) is only valid for the limit of incompressible flow because it is derived from Rossiter's equation by assuming that lag time is zero between the impact of a hydrodynamic structure on the trailing edge and the emission of an acoustic wave.

To compare the dependence of spectral peaks on cavity length with the frequency characteristics of self-sustained oscillations in laminar cavity flows, we calculated the local convection velocity (U_C) of pressure fluctuations from two-point time correlations (Fig. 15b). The overall distribution of convection velocity is very similar to the

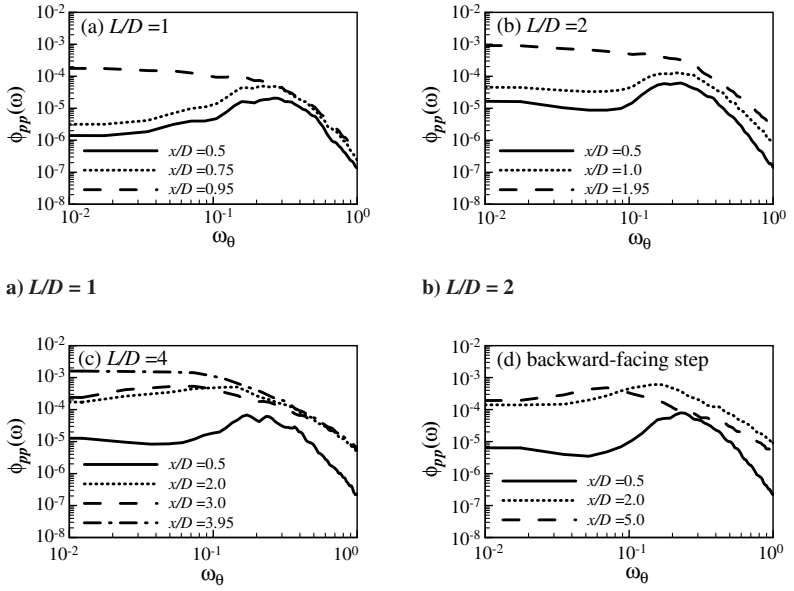

a) L/D = 1 **b) L/D = 2**

c) L/D = 4 **d) Backward-facing step**

Fig. 13 Frequency spectra of pressure fluctuations for various cavity lengths.

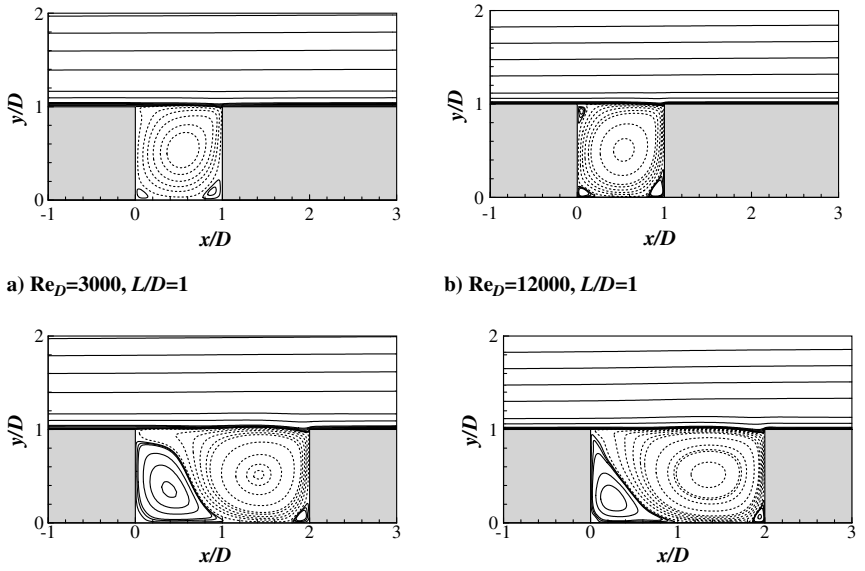

a) Re_D=3000, L/D=1 b) Re_D=12000, L/D=1

c) Re_D=3000, L/D=2 d) Re_D=12000, L/D=2

Fig. 14 Comparison of mean flow streamlines at $Re_D = 3000$ and 12,000.

previous result of Larchevêque et al. [5]. In the initial region, the convection velocity gradually increases with nearly constant acceleration. After the initial acceleration, the speed remains constant at about $0.6U_\infty$, which is slightly lower than $0.65U_\infty$ of Larchevêque et al. [5] and $0.66U_\infty$ of Ahuja and Mendosa [3]. When the shear layer approaches the trailing edge, the convection velocity rapidly decreases. Close examination of the time correlations indicates that the convection velocity is contaminated near the leading and trailing edges, as indicated by the dashed lines in Fig. 15b. In calculating the streamwise averaged convection velocity ($U_{C\text{avg}}$), which is needed to compare the peak frequency of Fig. 15a with the oscillating frequency of laminar cavity flows, the regions with contaminated convection velocities were excluded. The streamwise averaged convection velocities are calculated as $U_{C\text{avg}} = 0.475$ for $L/D = 1$ and $U_{C\text{avg}} = 0.490$ for $L/D = 2$. By substituting the convection velocities into Eq. (4), the peak frequencies of Fig. 15a are expressed as $fL/U_{C\text{avg}} = 2.08$ ($N = 2$) for $L/D = 1$ and $fL/U_{C\text{avg}} = 2.92$ ($N = 3$) for $L/D = 2$. The modes are exactly the same with the first and second eigenmodes of pressure fluctuations, which were reported in the proper orthogonal decomposition analysis of Lee et al. [24]. These findings indicate that the peak frequencies of the $Re_D = 12,000$ systems with $L/D = 1$ and 2 correspond to the second and third modes ($N = 2$ and 3), just like the oscillating frequency of laminar cavity flows [7]. Because Eq. (4) is originated from Rossiter's equation, Rossiter's mode is valid for predicting the self-sustained oscillations in incompressible cavity flows. Considering that the Nth modes are related to the streamwise wavelength (λ_x) of large-scale structures, the observation that the peak frequencies at $Re_D = 12,000$ for $L/D = 1$ and 2 correspond to the second and third modes suggests that large-scale vortical structures are present in turbulent cavity flows. Assuming that the streamwise length scale of pressure fluctuations is half of λ_x, the length scale is expected to be $0.4D$ near $x/D = 1.0$ when $L/D = 2$. Note that the streamwise length scale of pressure fluctuations is about $0.45D$ in the laminar case of Chang et al. [18], for which self-sustained oscillations are observed. The similarity of streamwise length scales supports the existence of large-scale vortical structures in turbulent cavity flows.

Next, to elucidate the large-scale vortical structures responsible for the Nth modes, we examined instantaneous flows for the system with a length-to-depth ratio of 2. Figures 16a and 16b show top and side views of the instantaneous coherent structures identified using the λ_2 criterion [25]. Identification using the λ_2 criterion shows only small vortical structures because λ_2 is calculated from the velocity gradient tensor. Nevertheless, the top view of λ_2 (Fig. 16a) shows a slight clustering of small vortical structures near $x/D = 0.8$ and in the vicinity of the trailing edge. The side view of λ_2 (Fig. 16b) shows the development of the shear layer, but fails to distinguish the large-scale vortical structures from the shear layer. Considering that the large-scale vortical structures were clearly identified in the laminar cavity flows of Gharib and Roshko [7] and Chang et al. [18], the obscurity of the vortical structures is attributed to turbulent characteristics of cavity flows. As seen in Fig. 16c, quasi-two-dimensional vortical structures are observed near $x/D = 0.8$ and in the vicinity of the trailing edge. In the region immediately downstream of the leading edge, another vortical structure is likely to be initiated. The large structures are more clearly observed in the contour plot of spanwise-averaged pressure fluctuations shown in Fig. 16d.

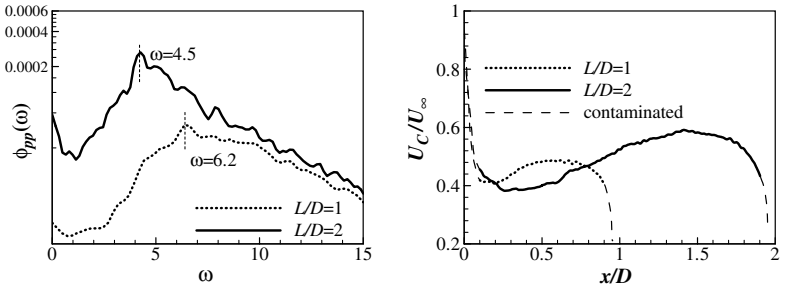

a) Frequency spectra b) Convection velocity

Fig. 15 Frequency spectra and convection velocity of pressure fluctuations when $Re_D = 12,000$. The convection velocity (U_C) is contaminated near the leading and trailing edges, as indicated by dashed lines in Fig. 15b.

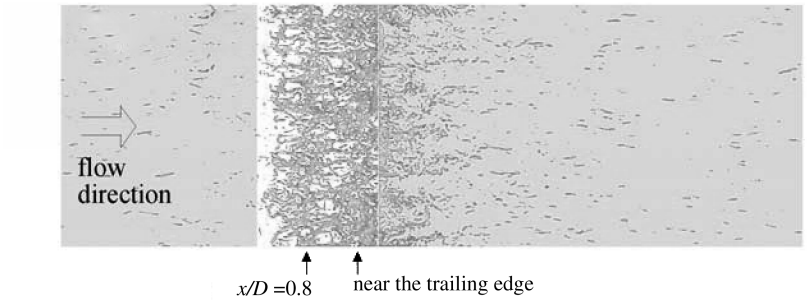

a) Top-view of λ_2

b) Side-view of λ_2

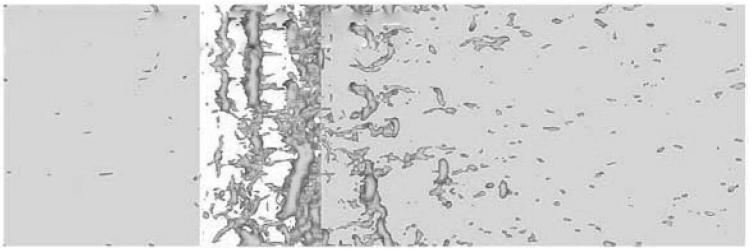

c) Top-view of instantaneous p′

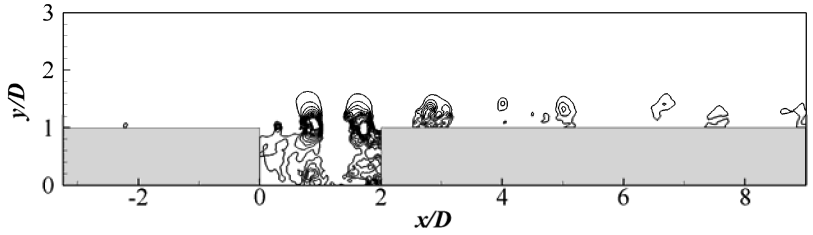

d) Spanwise average p′

Fig. 16 Instantaneous coherent structures: a) top view of λ_2 distribution, b) side view of λ_2 distribution, c) top view of p' distribution, and d) spanwise-averaged p'.

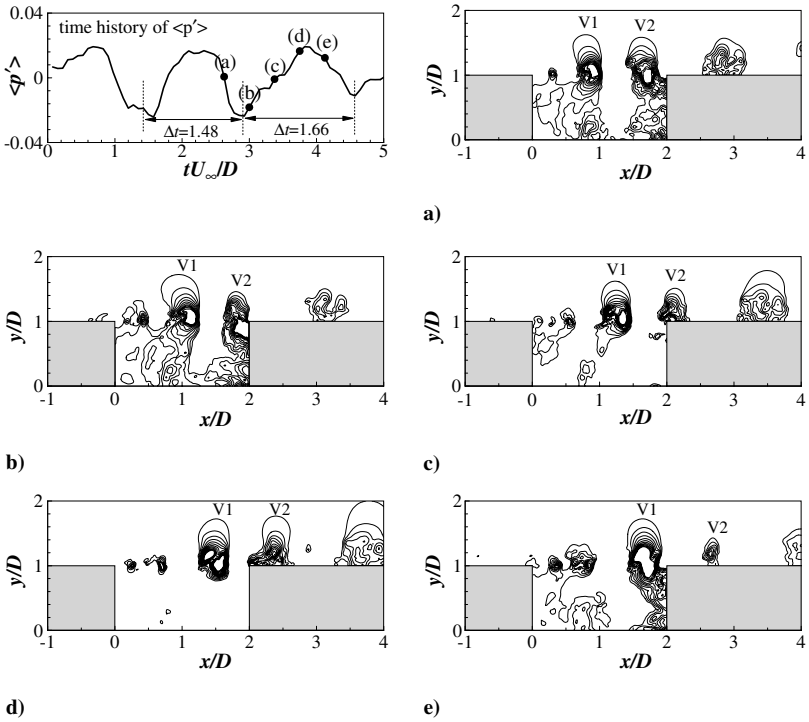

Fig. 17 Time history and sequential patterns of spanwise-averaged pressure fluctuations. Here, $\langle p' \rangle$ represents spanwise-averaged pressure fluctuations. Times of a)–e) are 2.625, 3.0, 3.375, 3.75, 4.125.

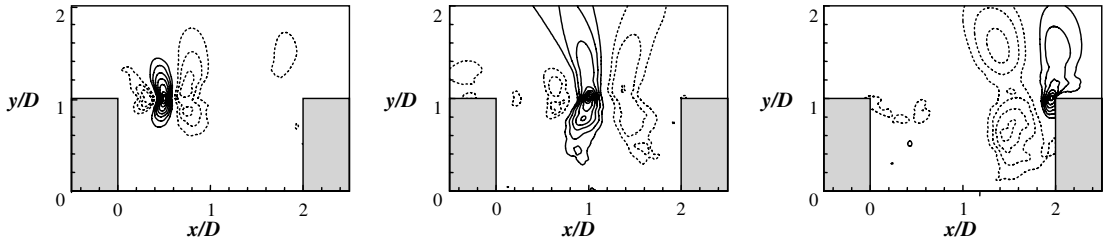

a) $X_0 = 0.5$ b) $X_0 = 1.0$ c) $X_0 = 1.95$

Fig. 18 Two-point correlations of pressure fluctuations with the following reference points: a) $(X_0, Y_0) = (0.5, 1.0)$, b) $(X_0, Y_0) = (1.0, 1.0)$, and c) $(X_0, Y_0) = (1.95, 1.0)$. Here solid and dotted lines represent positive and negative correlations, respectively.

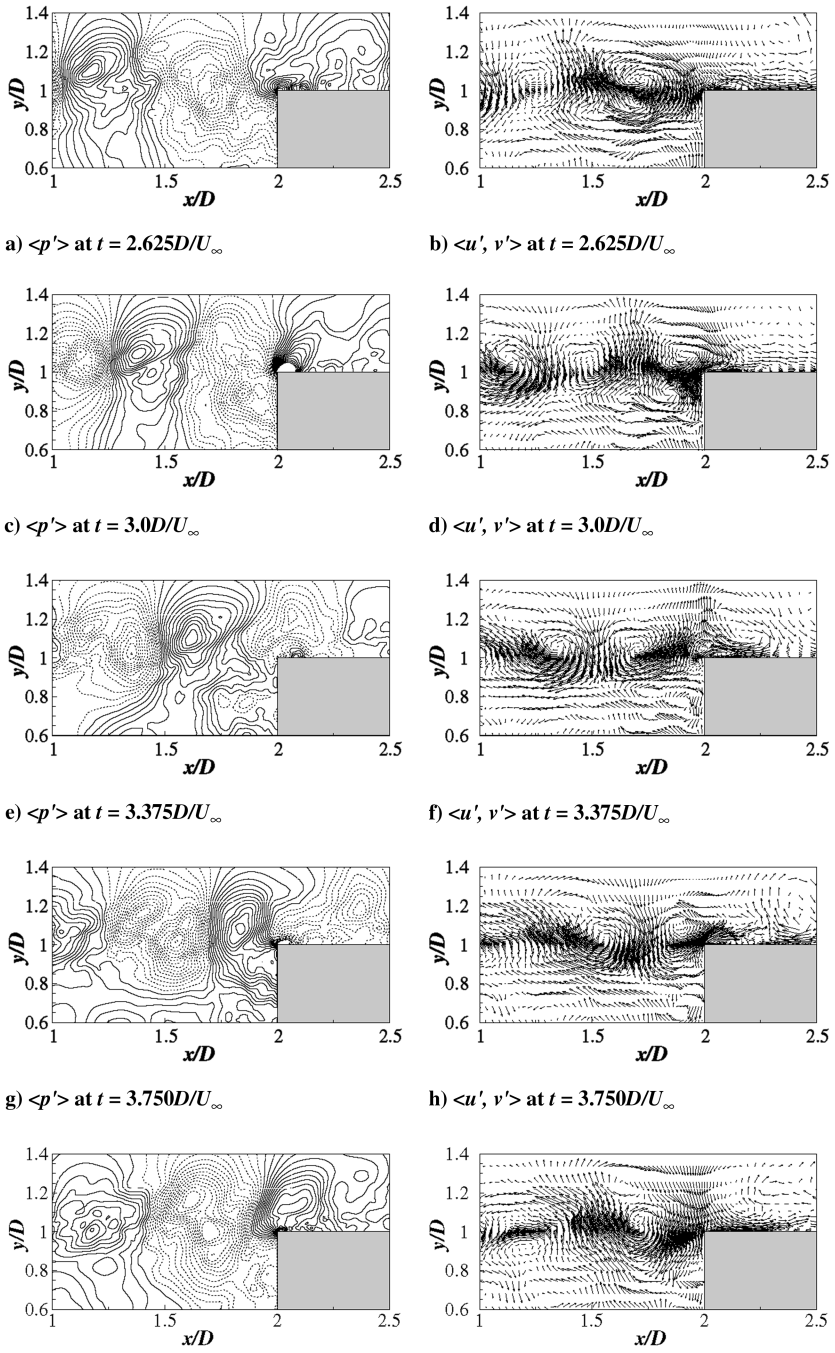

a) $<p'>$ at $t = 2.625D/U_\infty$ b) $<u', v'>$ at $t = 2.625D/U_\infty$

c) $<p'>$ at $t = 3.0D/U_\infty$ d) $<u', v'>$ at $t = 3.0D/U_\infty$

e) $<p'>$ at $t = 3.375D/U_\infty$ f) $<u', v'>$ at $t = 3.375D/U_\infty$

g) $<p'>$ at $t = 3.750D/U_\infty$ h) $<u', v'>$ at $t = 3.750D/U_\infty$

I) $<p'>$ at $t = 4.125D/U_\infty$ j) $<u', v'>$ at $t = 4.125D/U_\infty$

Fig. 19 Sequential patterns of spanwise-averaged pressure fluctuations and velocity fluctuations. Here, $\langle p' \rangle$ represents spanwise-averaged pressure fluctuations and $\langle u', v' \rangle$ represents a vector of spanwise-averaged velocity fluctuations. Solid and dotted lines of pressure fluctuations represent positive and negative values, respectively.

Figure 17 shows the time history and sequential patterns of the spanwise-averaged pressure fluctuations. The time history records the spanwise-averaged pressure fluctuations measured at $(x/D, y/D) = (1.0, 1.0)$. The pressure fluctuations show quasi-periodic oscillations in the range of $1.4 \leq \Delta t \leq 1.7$, where Δt is the time interval between consecutive large-scale structures. The peak frequency ($\omega_{\text{peak}} = 4.5$) of the energy spectra is in good agreement with the range of the time interval. The sequence of contour plots in Figs. 17a–17e show the convective patterns of the large-scale vortical structures. In Fig. 17a, "V1" indicates a large-scale vortical structure centered near $x/D = 0.8$, whereas "V2" represents another vortical structure near the trailing edge. Inspection of the time history shows that, at the time corresponding to Fig. 17a ($t = 2.625D/U_\infty$), the pressure fluctuations at the measurement point, $(x/D, y/D)$= $(1.0, 1.0)$, change from positive to negative. This change can be attributed to the downstream convection of V1 toward the measurement point. At the time when the center of V1 coincides with the measurement point, as shown in Fig. 17b, the pressure shows very strong negative fluctuations. As V2 convects downstream, it impinges on the trailing edge of the cavity. The contour plot at $t = 3.375D/U_\infty$ (Fig. 17c) shows partial clipping of V2 and continuous convection of V1. A small part of the clipped V2 is entrained into the cavity along the vertical wall, while the majority is ejected out of the cavity [10]. At $t = 3.750D/U_\infty$ (Fig. 17d), strong positive pressure fluctuations are observed at $(x/D, y/D) = (1.0, 1.0)$ due to a secondarily induced rotation by adjacent vortical structures, and complete escape of V2 from the cavity is observed. At $t = 3.375D/U_\infty$ (Fig. 17e), V1 is situated at almost the same location as V2 was in Fig. 17a, and another vortical structure appears to be forming near $x/D = 0.8$. After escaping from the cavity, V2 gradually dissipates as it is advected along the downstream wall. As seen in each figure, the vortical structures are small near the leading edge but increase in size as they convect toward the trailing edge.

To quantify the length scales of the vortical structures, we examined two-point correlations of pressure fluctuations of the following form:

$$R_{\phi\phi}(x/D, y/D; X_0, Y_0) = \frac{\langle \phi(X_0, Y_0, z, t)\phi(x/D, y/D, z, t)\rangle}{\phi_{\text{rms}}(X_0, Y_0)\phi_{\text{rms}}(x/D, y/D)} \quad (5)$$

where (X_0, Y_0) represents a reference point. Figure 18 shows the results obtained using three streamwise locations as the reference point: $x/D = 0.5$, 1.0 and 1.95. In this figure, solid and dotted lines represent positive and negative correlations, respectively. The streamwise length scale of the vortical structures is about $0.2D$ when the vortical structures are observed near $x/D = 0.5$ (Fig. 18a). On moving downstream, the vortical structure grows such that it has a length scale of $0.4D$ at $x/D = 1.0$ (Fig. 18b). These length scales are consistent with the predicted length scales based on the peak frequency of the energy spectra and the convection velocity of the pressure fluctuations. When the vortical structures impinge on the trailing edge (Fig. 18c), the streamwise length scale of the structures diminishes due to the interaction of the structures with the cavity walls. Note that the pressure fluctuations at $y/D = 1$ are almost uncorrelated with those at the bottom wall ($y/D = 0$) inside the cavity. These findings indicate that experimental measurements of the pressure fluctuations on the bottom wall inside the cavity are of little use when attempting to elucidate the behavior of pressure fluctuations along the lip line of the cavity.

Figure 19 shows a sequence of plots displaying the time evolution of the large-scale vortical structures as they impinge on the trailing edge. Here, $\langle p' \rangle$ and $\langle u', v' \rangle$ represent spanwise-averaged pressure fluctuations and vectors of spanwise-averaged velocity fluctuations, respectively. Solid and dotted lines represent negative and positive values in the contour plots of $\langle p' \rangle$. As seen in Figs. 19a and 19b, the negative pressure fluctuations and clockwise rotating structures near $(x/D, y/D) = (1.7, 1.0)$ represent the vortical structures corresponding to V2 of Fig. 17. For $t = 2.625D/U_\infty$, the fringe of V2 begins to impinge on the trailing edge, although positive pressure fluctuations are observed on the trailing edge. By $t = 3.0D/U_\infty$ (Fig. 19d), the large-scale vortical structure V2 has been clipped by the trailing edge of the cavity. As briefly discussed in relation to Fig. 17, a small portion of the clipped V2 is entrained into the cavity along the vertical wall while the majority is ejected out of the cavity. As time progresses to $t = 3.375D/U_\infty$ (Figs. 19e and 19f), the entrained part of V2 weakens as it moves along the vertical wall. Meanwhile, the ejected part retains a large-scale vortical structure with strong negative pressure fluctuations. At the later times of $t = 3.750D/U_\infty$ (Figs. 19g and 19h), the entrained part of V2 is no longer observed. The vectors in Fig. 19h indicate that a counter-clockwise rotation with positive pressure fluctuations is induced by two vortical structures: one is the escaping part of V2 and the other is an incoming vortical structure corresponding to the V1 vortical structure of Fig. 17. Although some variations in the behavior of the vortical structures can be observed in the full time history, the results clearly show that the partial clipping of large-scale vortical structures

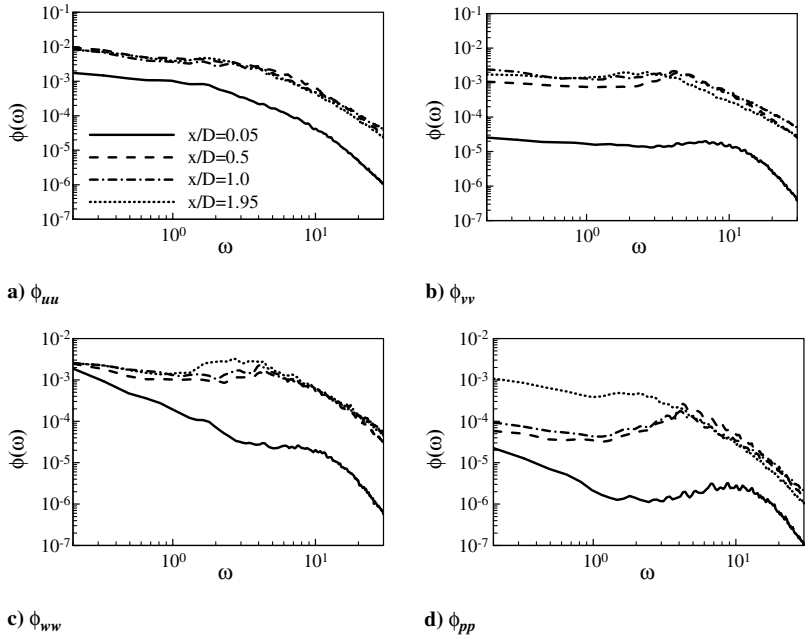

Fig. 20 Energy spectra of fluctuating quantities at several streamwise locations between the leading edge ($x/D = 0$) and the trailing edge ($x/D = 2$) along the lip line ($y/D = 1$) of the cavity geometry. Here the length-to-depth ratio is 2 and $Re_D = 12,000$.

described herein is the main process during impingement on the trailing edge.

Figure 20 shows energy spectra of fluctuating quantities at several streamwise locations between the leading edge ($x/D = 0$) and the trailing edge ($x/D = 2$) along the lip line ($y/D = 1$) of the cavity geometry, for a system with $L/D = 2$ and $Re_D = 12,000$. With the exception of the energy spectra of the pressure fluctuations, the energy spectra do not clearly show dominant spectral peaks corresponding to the shedding and impinging of the vortical structures that were clearly observed in the contour plots of instantaneous and spanwise-averaged pressure fluctuations (Fig. 17), as well as in the vectors of spanwise-averaged velocity fluctuations (Fig. 19). In the energy spectra of streamwise velocity fluctuations (Fig. 20a), no spectral peak is observed. Meanwhile, in the energy spectra of vertical and spanwise velocity fluctuations (Figs. 20b and 20c), slight energetic increases are observed in the vicinity of $\omega = 4.5$ but it is difficult to determine the peak frequency in the broad spectra. These findings are consistent with the results of Ashcroft and Zhang [17], who found that two-point correlations of vertical velocity exhibited a pattern of alternating regions of positive and negative values reflecting the organized nature of the coherent structures within the shear layer, but that the correlations of the streamwise velocity showed no evidence of these coherent structures. Grace et al. [15] also observed no spectral peaks in the power spectra density of streamwise velocity although their experiments were carried out by placing hot wires at a number of streamwise locations. While the velocity fluctuations are inadequate to describe the spectral characteristics of self-sustained oscillations, the spectral peaks of $\omega = 4.5$ are observed in the energy spectra of pressure fluctuations as shown in Fig. 20d. The peak frequencies correspond to the shedding frequencies of large-scale vortical structures in the central region of $x/D = 0.5$ and 1.0. However, the peak frequency is not observed near the leading edge ($x/D = 0.05$) due to the lack of large-scale vortical formation or near the trailing edge ($x/D = 1.95$) due to the impingement of vortical structures [26].

VI. Conclusions

In the present study we performed DNSs and LESs of incompressible turbulent flows over deep and shallow cavities in the range of $600 \leq Re_D \leq 12,000$ to investigate the influence of the incoming turbulent boundary layer on self-sustained oscillations of the shear layer. When the turbulent boundary layer approached the leading edge in cavity flows with $Re_D = 600$ and 3000, the energy spectra of pressure fluctuations showed spectral peaks in the range of $0.15 \leq \omega_\theta \leq 0.3$. Examination of conditionally averaged flowfields revealed that high-speed streaky structures in the incoming turbulent boundary layer made the separated shear layer locally unstable and generated the pressure fluctuations with the spectral peaks. As the flow moved downstream over shallow cavities, however, the streaky structures were disturbed and the spectral peaks were no longer observed. Instead of the streaky structures, large-scale vortical structures were observed to form via a mechanism analogous to vortical shedding of a backward-facing step flow, but the development of these large-scale vortical structures was impeded by the trailing edge of the cavity. Inspection of the time evolution of spanwise-averaged pressure fluctuations revealed that the shedding of the large-scale vortical structures is irregular in shallow cavities. Considering that self-sustained oscillations are meaningful only when the oscillations arise from a geometric singularity of the cavity, neither the energetic pressure fluctuations generated by the high-speed streaky structures nor the irregular shedding of large-scale vortical structures are regarded as self-sustained oscillations in the incompressible turbulent flow over an open cavity. In the turbulent cavity flow with $Re_D = 12,000$, the peak frequencies of the energy spectra at cavity lengths of $L/D = 1$ and 2 were found to correspond to the Nth modes with $N = 2$ and 3, respectively. While the vortex identification based on λ_2 revealed a slight clustering of small vortical structures in the vicinity of the large-scale vortical structures, inspection of the instantaneous pressure fluctuations as well as spanwise-averaged pressure fluctuations made it clear that regular shedding of quasi-two-dimensional vortical structures was responsible for the peak frequency in the energy spectra. When the large-scale vortical structure impinged on the trailing edge, the structure split into a small part entrained into the cavity along the vertical wall and a large part that was ejected out of the cavity. The characteristics revealed in the present work, particularly the regular shedding and impinging of large-scale vortical structures, strongly suggest that a fully turbulent boundary layer can give rise to self-sustained oscillations in an incompressible turbulent flow over an open cavity. This is consistent with the previous results that a large value of D/θ is essential for the onset of self-sustained oscillations because the shear layer amplification is strongly dependent on D/θ.

Acknowledgment

This work was supported by the Creative Research Initiatives (Center for Opto-Fluid-Flexible Body Interaction) of the Ministry of Education, Science & Technology/National Research Foundation of Korea.

References

[1] Norton, D. A., "Investigation of B47 Bomb Bay Buffet," Boeing Airplane Co. Document No. D12675, 1952.

[2] Rossiter, J. E., "Wind-Tunnel Experiments on the Flow Over Rectangular Cavities at Subsonic and Transonic Speeds," Aeronautical Research Council Reports and Memoranda No. 3438, 1964.

[3] Ahuja, K., and Mendosa, J., "Effects of Cavity Dimensions, Boundary Layer and Temperature on Cavity Noise with Emphasis on Benchmark Data to Validate Computational Aeroacoustics Codes," NASA Final Report Contract 19061, Task 13, 1995.

[4] Rowley, C. W., Colonius, T., and Basu, A. J., "On Self-Sustained Oscillations in Two-Dimensional Compressible Flow Over Rectangular Cavities," *Journal of Fluid Mechanics*, Vol. 455, 2002, pp. 315–346. doi:10.1017/S0022112001007534

[5] Larchevêque, L., Sagaut, P., Lê, T. H., and Comte, P., "Large-Eddy Simulations of a Compressible Flow in a 3D Open Cavity at High Reynolds Number," *Journal of Fluid Mechanics*, Vol. 516, 2004, pp. 265–301. doi:10.1017/S0022112004000709

[6] Sarohia, V., "Experimental Investigation of Oscillations in Flows Over Shallow Cavities," *AIAA Journal*, Vol. 15, No. 7, 1977, pp. 984–991. doi:10.2514/3.60739

[7] Gharib, M., and Roshko, A., "The Effect of Flow Oscillations on Cavity Drag," *Journal of Fluid Mechanics*, Vol. 177, 1987, pp. 501–530. doi:10.1017/S002211208700106X

[8] Rockwell, D., and Naudascher, E., "Review—Self-Sustaining Oscillations of Flow Past Cavities," *Journal of Fluids Engineering*, Vol. 100, 1978, pp. 152–165.

[9] Rockwell, D., and Naudascher, E., "Self-Sustained Oscillations of Impinging Free Shear Layer," *Annual Review of Fluid Mechanics*, Vol. 11, 1979, pp. 67–94. doi:10.1146/annurev.fl.11.010179.000435

[10] Rockwell, D., and Knisely, C., "The Organized Nature of Flow Impingement Upon a Corner," *Journal of Fluid Mechanics*, Vol. 93, 1979, pp. 413–432. doi:10.1017/S0022112079002573

[11] Burroughs, C. B., and Stinebring, D. R., "Cavity Flow Tones in Water," *Journal of the Acoustical Society of America*, Vol. 95, No. 3, 1994, pp. 1256–1263. doi:10.1121/1.408568

[12] Howe, M. S., "Low Strouhal Number Instabilities of Flow Over Apertures and Wall Cavities," *Journal of the Acoustical Society of America*, Vol. 102, No. 2, 1997, pp. 772–780. doi:10.1121/1.419903

[13] Pereira, J. C. F., and Sousa, J. M. M., "Experimental and Numerical Investigation of Flow Oscillations in a Rectangular Cavity," *Journal of Fluids Engineering*, Vol. 117, 1995, pp. 68–74. doi:10.1115/1.2816825

[14] Lin, J. -C., and Rockwell, D., "Organized Oscillations of Initially Turbulent Flow Past a Cavity," *AIAA Journal*, Vol. 39, No. 6, 2001, pp. 1139–1151. doi:10.2514/2.1427

[15] Grace, S. M., Dewar, W. G., and Wroblewski, D. E., "Experimental Investigation of the Flow Characteristics Within a Shallow Wall Cavity for Both Laminar and Turbulent Upstream Boundary Layers," *Experiments in Fluids*, Vol. 36, 2004, pp. 791–804.

doi:10.1007/s00348-003-0761-3
[16] Chatellier, L., Laumonier, Y., and Gervais, Y., "Theoretical and Experimental Investigations of Low Mach Number Turbulent Cavity Flows," *Experiments in Fluids*, Vol. 36, 2004, pp. 728–740. doi:10.1007/s00348-003-0752-4
[17] Ashcroft, C., and Zhang, X., "Vortical Structures Over Rectangular Cavities at Low Speed," *Physics of Fluids*, Vol. 17, 2005, p. 015104. doi:10.1063/1.1833412
[18] Chang, K. C., Constantinescu, G., and Park, S. -O., "Analysis of the Flow and Mass Transfer Processes for the Incompressible Flow Past an Open Cavity with a Laminar and a Fully Turbulent Incoming Boundary Layer," *Journal of Fluid Mechanics*, Vol. 561, 2006, pp. 113–145. doi:10.1017/S0022112006000735
[19] Kim, K., Baek, S. -J., and Sung, H. J., "An Implicit Velocity Decoupling Procedure for the Incompressible Navier–Stokes Equations," *International Journal for Numerical Methods in Fluids*, Vol. 38, No. 2, 2002, pp. 125–138. doi:10.1002/fld.205
[20] Lund, T. S., Wu, X., and Squires, K. D., "Generation of Turbulent Inflow Data for Spatially-Developing Boundary Layer Simulation," *Journal of Computational Physics*, Vol. 140, 1998, pp. 233–258. doi:10.1006/jcph.1998.5882
[21] Germano, M., Piomelli, U., Moin, P., and Cabot, W. H., "A Dynamic Subrid-Scale Eddy Viscosity Model," *Physics of Fluids A*, Vol. 3, 1991, pp. 1760–1765. doi:10.1063/1.857955
[22] Le, H., Moin, P., and Kim, J., "Direct Numerical Simulation of Turbulent Flow Over a Backward-Facing Step," *Journal of Fluid Mechanics*, Vol. 330, 1997, pp. 349–374. doi:10.1017/S0022112096003941
[23] Kiya, M., and Sasaki, K., "Structure of Large-Scale Vortices and Unsteady Reverse Flow in the Reattaching Zone of a Turbulent Separation Bubble," *Journal of Fluid Mechanics*, Vol. 154, 1985, pp. 463–491. doi:10.1017/S0022112085001628
[24] Lee, S. B., Kang, W., and Sung, H. J., "Organized Self-Sustained Oscillations of Turbulent Flows Over an Open Cavity," *AIAA Journal*, Vol. 46, No. 11, 2008, pp. 2848–2856. doi:10.2514/1.36860
[25] Jeong, J., and Hussain, F., "On the Identification of a Vortex," *Journal of Fluid Mechanics*, Vol. 285, 1995, pp. 69–94. doi:10.1017/S0022112095000462
[26] Kang, W., Lee, S. B., and Sung, H. J., "Self-Sustained Oscillations of Turbulent Flows Over an Open Cavity," *Experiments in Fluids*, Vol. 45, 2008, pp. 693–702. doi:10.1007/s00348-008-0510-8